Proceedings: 2nd International Symposium on Performance Enhancement for Marine Applications

October 14-16, 1990
Newport, Rhode Island

COMPUTATIONAL MODELING OF CAVITATION

C. W. Hirt

Flow Science, Inc.
1325 Trinity Drive
Los Alamos, New Mexico 87544
USA

July 1990

ABSTRACT

Flows around high speed bodies in water are subject to cavitation. In general, cavitation is to be avoided because it represents a loss of useful energy and can result in structural damage. In some cases, however, controlled cavitation can be beneficial. For instance, a thin supercavitation bubble surrounding a torpedo may reduce skin friction drag, or cavitation can be used in underwater acoustic generators.

In this paper a new computational model is described that has been implemented in a commercial computer program that produces transient, three-dimensional solutions of the Navier-Stokes equations.

Examples are presented that cover a wide range of applications involving cavitation phenomena. These include sloshing, flows over torpedo-shaped bodies, and water surface reentry problems. Comparisons with experimental data have been made for those examples where suitable data is available.

INTRODUCTION

Cavitation is associated with the appearance of vapor or gas bubbles in flowing liquids.[1] As a rule, cavitation is the term used when vapor or gas bubbles develop because of a lowering of the fluid pressure. Boiling, on the other hand, is usually the term used to describe the appearance of bubbles when the temperature of the fluid is raised. In either case the molecular processes are the same; dissolved gases come out of solution and/or the liquid undergoes a liquid-to-vapor phase change. In practice, the possibility of cavitation is usually characterized by a Cavitation Number,

$$K = (p_o - p_c) / \left(\frac{1}{2}\rho u^2\right)$$

where p_o is some reference pressure, p_c is the vapor pressure and u is some reference velocity.

Most often cavitation is to be avoided because it is a sink of energy and may even result in structural damage. However, in some cases controlled cavitation may be useful, for instance, in reducing skin friction drag on high speed torpedos or for inducing locally high pressures/temperatures for certain chemical reactions in liquid mixtures.[2]

In this paper we describe a new cavitation model that has been added to the commercial FLOW-3D computer program.[3] The model is most useful for supercavitating flows, that is, for flows where the cavitation bubbles become large enough to be easily resolved by one or more cells within a computational grid.

This new model makes use of an existing bubble-void model in FLOW-3D but differs from that model in several important ways. Most importantly, in cavitation we require a mechanism for the automatic formation of new bubbles when the pressure falls below a specified level (i.e., below the cavitation or saturation pressure). Conversely, cavitation bubbles can disappear when the surrounding pressure exceeds the saturation pressure. We shall see in the illustrative examples why this distinction is crucial.

MODELING CONSIDERATIONS

The FLOW-3D Program

The computational platform for this work is a commercial program, FLOW-3D, marketed by Flow Science, Inc. FLOW-3D, which can be purchased, leased, or accessed at computer service bureaus, is a general purpose fluid flow and heat transfer package.

The FLOW-3D program is based on a finite-difference solution algorithm for the three-

dimensional, time-dependent Navier-Stokes equations. A novel feature of the code is its ability to represent extremely complicated flows containing one or more free surfaces. This feature, which is based on the Volume-of-Fluid (VOF) computational technique,[4] is essential for modeling supercavitation phenomena.

Free surfaces in the present context are treated as sharp interfaces separating liquid and gas regions. The gas regions in FLOW-3D can be regions of fixed pressure (i.e., regions having no inertia and connected to "infinite" reservoirs capable of keeping the gas pressure at a constant value). Alternatively, the gas regions in FLOW-3D can be finite regions in which an adiabatic γ-law pressure/volume relation exists.

The code does not have a capability to simultaneously model the dynamics of both gas and liquid or to model dispersed two-phase mixtures of gas and liquid. This is an important limitation with respect to cavitation. For instance, it means that the cavitation model to be described is primarily for supercavitating situations where cavitation bubbles are large enough to be resolved by the computational grid. It also means that these "bubbles" are treated as constant pressure regions once they are identified in the computations.

No details of the basic computational algorithm are given here. Reference 4 should be consulted for this purpose as it describes the general computational approach used in FLOW-3D.

Assumptions and Approximations

A number of simplifying assumptions have been made in adding the new cavitation model to FLOW-3D. First, we assume that the liquid is incompressible and that the exchange of vapor (or gas) with the liquid is sufficiently rapid that bubbles always have pressures equal to the cavitation pressure. In particular, a change in volume of a cavitation bubble does not change its pressure. When a computational grid cell has a pressure below the cavitation pressure, a vapor bubble must be allowed to form. This formation is modeled by allowing the velocity divergence to become positive by an amount proportional to how far the pressure is below the cavitation pressure,

$$\nabla \cdot \vec{u} = -(p - p_c)/\tau \qquad (1)$$

where p_c is the cavitation pressure (a constant) and τ is a relaxation time. The rate of formation has a time constant that is approximately equal to five computational time steps, i.e., $\tau = 5\delta t$. In effect, this allows more fluid to flow out of a computational grid cell than is consistent with the assumption of incompressibility. When this happens a void region begins to develop, but it is not identified as a distinct void region in the code until it reaches a size large enough to occupy at least one entire computational cell.

The vapor production rate, Eq. (1), is only active during the initial formation of a vapor bubble. Once the liquid volume fraction of a cell is below 0.99, the cell pressure is then fixed at the cavitation pressure. Cells within the fluid and having a volume fraction less than 0.99 are treated as fixed pressure cells. These cells will have, in general, nonzero velocity divergences.

It should be emphasized that vapor cannot have a velocity different from that of the liquid. Furthermore, in large vapor regions that are resolved by the grid there is no vapor momentum as these regions are modeled strictly as regions of constant pressure. In other words, the current cavitation model is not a complete two-phase flow model. This is an important approximation that must be kept in mind when using FLOW-3D to model cavitation phenomena. One example of this limitation will be pointed out in connection with an example of supercavitation behind a circular disk.

Limitations

Since p_c is an absolute pressure, it is important to define computational problems that have some reference pressure set either through an existing free surface pressure or through a specified boundary pressure.

It is possible to initialize problems with free surface (gas) pressures that are different from the cavitation pressure as long as this pressure is not less than the cavitation pressure. Such void regions will maintain their pressures using the code's void-pressure models as long as they remain distinct regions. Of course, any void region, whether a cavitation bubble or not, that intersects a specified pressure boundary will immediately have the same pressure as the boundary since the boundary is assumed connected to an infinite reservoir.

Finally, we should note that the cavitation model is not allowed to operate during the first five time cycles of a calculation. This restriction gives time for inconsistent or arbitrary initial pressures to settle down to realistic values before any tests for cavitation are made. For example, in the flow around a disk example described below, the initial impulsive start given to the flow introduces extreme and unrealistic pressure transients that last for two or three computational time cycles.

ILLUSTRATIVE PROBLEMS

In this section we describe several example problems that illustrate the capabilities of the new model. We begin with cavitation originating at a constriction in a pipe.

Cavitation in a Constricted Pipe

Figure 1 shows a sketch of the problem we wish to solve. Non-dimensional units are used in which the pipe diameter is 1.0 unit. At the constriction the minimum flow area is 36% of the full pipe area. A uniform flow of incompressible liquid with unit velocity is specified at the upstream boundary of the pipe. The fluid density is 1.0 and is assumed to have a low enough viscosity to be treat as inviscid. The outflow boundary is specified as a constant pressure boundary with a pressure of 10.0.

Bernoulli's relation indicates a pressure reduction at the constriction of about 3.86. This suggests that the setting of a cavitation pressure slightly above 6.14 should result in a relatively small region of cavitation.

Figure 2 shows a time sequence of computed results obtained with the FLOW-3D program. For this calculation 10 mesh zones were used to resolve the pipe radius and 50 zones were used axially. The zone size was smallest in the region of the constriction in order to better resolve any cavitation that might occur. (The plots show a full cross section, but only one symmetric half was actually computed.)

The computed results indicate an unsteady flow with a cavitation bubble initially growing from the pipe wall at a location slightly downstream from the maximum constriction. The cavitation bubble grows rapidly at first, reaches a maximum size, then collapses. This growth and collapse process repeats itself in a cyclic manner.

Although it was originally anticipated that a steady flow result would be computed, there is experimental confirmation for this type of unsteady behavior.[5] For instance, Fig. 3 shows a series of frames from a motion picture taken of cavitating flow in a constricted pipe similar to that used in the computations. This figure has been reproduced from page 84 of Ref. 5.

An explanation of why the flow is cyclic can be obtained from an examination of the computed results. Cavitation first develops at the pipe wall, just downstream from the minimum area, where the pressure is a minimum. As the cavitation vapor bubble grows, the flow separates from the pipe wall leaving a region of relatively slow flow near the wall in the wake of the bubble, see Fig. 4.

Downstream from the constriction there must be some pressure recovery as the flow spreads out over the full pipe cross section. When this happens there is an adverse pressure gradient along the pipe wall that drives flows back upstream into the vapor bubble. Eventually the reverse flow causes the bubble to completely collapse.

After the collapse there is a short period while the flow adjusts to its new state (i.e., no flow separation immediately downstream of the constriction) before beginning the growth of a new vapor bubble.

This example is a good illustration of the usefulness of computational modeling. As previously mentioned, we had anticipated a steady flow result, but an examination of the computed result provides a ready explanation for the unsteady behavior that was obtained. Of course, the subsequent uncovering of experimental confirmation is comforting, particularly when using a newly developed computational model!

Two general observations about this example are worth noting. First, the initial formation of the vapor bubble is a result of Eq. (1), which allows for a nonzero velocity divergence (i.e., vapor production). The computed results cannot otherwise be duplicated with the constant pressure bubble model that was originally in the FLOW-3D program.

Secondly, when the cavitation pressure is sufficiently increased, resulting in a large enough vapor bubble to reach the outflow boundary, the problem changes in a fundamental way. If the bubble reaches the downstream boundary, it must assume the pressure of the boundary which is assumed connected to a fixed pressure reservoir. Once this happens, the computational problem cannot recover to a pure vapor bubble situation.

The computational (CPU) time required for a problem time of 15.0 units was 3.8 hours on a MicroVAX II computer. This time period covered several oscillations of the growth and collapse of the cavitation bubble.

Cavitation Behind a Circular Disk

This example was selected as a test case because there exists some qualitative experimental data with which to make a comparison. Unfortunately, the data consists of a single photograph, Plate 18, from the book FLUID DYNAMICS by G. K. Batchelor.[6] Nevertheless, the photograph is clear and does provide a useful benchmark test.

The problem consists of a thin circular disk mounted on an axisymmetric rod that extends rearward with respect to the flow, see Fig. 5. The physical conditions for this problem are specified in terms of the nondimensional parameter K=0.19, the cavitation number. Since only this nondimensional number was given, we have used dimensionless quantities to define our computational model; i.e., a disk diameter of 1.0, a flow speed of 1.0, and a fluid density of 1.0. The cavitation pressure was set at 0.0, which leaves the ambient pressure to be chosen to give the desired cavitation number, $p_o=K/2$, or in this example $p_o=0.095$.

Computational Model

A mesh consisting of 20 radial cells and 50 axial cells was used to define the computational region that had a radius of 2.0 and a length of 7.5 units. The disk was modeled with the baffle capability in FLOW-3D, while the support rod was defined as an obstacle. The rod's diameter was guessed to be 0.4 times the disk diameter (an accurate measurement from the photo was not possible, but it is

unlikely that the exact diameter is important). A constant axial flow of unit magnitude was specified to enter the bottom of the mesh. At the outer radial side and the top (outflow) boundaries a constant ambient pressure condition was used.

Computational Results

Development of the vapor region with time is illustrated in Fig. 6. In these plots a full cross section is plotted even though only one symmetric half is actually computed. The flow is started impulsively and the cavity immediately begins to grow behind the outer edge of the disk. By t=6.0 the outer surface of the cavity is essentially stationary in time except for the base region where the flow closes on the support rod. This can be seen, for example, by observing that the upstream portion of the cavity at t=6.0 is nearly identical with that at t=10.0 in Fig. 7.

A comparison with data is also given in Fig. 7 where the bold black dots indicate the location of the cavity boundary as measured from the Batchelor photograph. Excellent agreement is observed over most of the cavity.

In a preliminary calculation using a coarser grid, the radial diameter of the cavity was slightly underpredicted. To obtain agreement it was necessary to increase the resolution near the edge of the disk in order to get the proper angle for flow leaving the edge.

The most interesting region is at the rear end of the cavity. This region is not stationary as can be seen by comparing the Fig. 7 result with the flow configuration at t=20.0 shown in Fig. 8. It is interesting to note Batchelor's remarks about the experimental observation of this region.[6] He states (p. 505):

> "Some of the photographs of cavities attached to bodies with K>0 do suggest that there is a tendency for the cavity to be filled up from the rear with a foaming mass of water and then for the contents of the cavity to be swept downstream suddenly with repetition of the whole process."

In our computation we see that where the flow around the outer surface of the cavity closes on the central rod there is a flow stagnation point. Some fluid at this point is directed back toward the rear of the disk. Since there is no pressure gradient or any other resistive force in this region, the flow will eventually hit the rear surface of the disk.

In Fig. 8 this re-entrant flow has only progressed about halfway toward the disk, and some of this fluid is interacting with the outer surface of the cavity. The pressure contours in Fig. 8 indicate there is virtually no pressure variation within the cavity. A very small negative pressure exists within the re-entrant fluid, but this is producing more vapor and does not last for long.

It is important to recognize that some physical phenomena have been neglected in the computer simulation that could influence the behavior of the re-entrant flow. For instance, no turbulence effects (or even viscous effects) were included in the calculation. Perhaps more important is the fact that no vapor dynamics are included. It is likely, and experiments tend to support the idea, that vapor is continually leaving the cavity surface and flowing toward the rear of the cavity. Momentum of the vapor could act as an axial force that confines the re-entrant flow to the rear portion of the cavity. It would be interesting to know, for example, whether or not fluid is actually observed to strike the rear of the disk. Answers to such questions will have to wait until further experimental data is available.

This calculation, out to a problem time of t=20.0, required 3.69 hours of CPU time on a MicroVAX II computer. If only the basic cavity is of interest, the calculation could have been terminated at t=10.0, thus cutting the CPU time in half.

Cavitation about a Torpedo

In this third example we consider flow about the body of a torpedo. The torpedo consists of a cylindrical piece with a conical nose that is 45 cm long from nose to base and has a diameter of 10 cm. Since the torpedo is moving at "high speed," 10,000 cm/s (100 m/s), we expect to observe some cavitation. Figure 9 shows a schematic of the problem. The ambient pressure has been taken to be 2.0 atm and the cavitation pressure is P_c=0.03 atm.

Computational Model

The computational mesh consisted of 25 radial cells and 42 axial cells to define a radial region of 25 cm and an axial region of 75 cm. As in the previous case, the outer radial boundary is a specified pressure boundary, but now the outflow boundary is continuative (i.e., zero normal derivatives for all flow quantities). At the inflow the velocity is held at a constant value of 10,000 cm/s. We assume the torpedo is subjected to an impulsive start. The total computational problem time was set to be 10 ms, which is sufficient to achieve steady state conditions.

Computational Results

Snapshots of the computed flow are collected in Fig. 10. In this case we see that two cavitation bubbles form, one rearward of the nose/body intersection and one at the outer edge of the base. These two bubbles eventually merge into a single bubble leaving some fluid inside the cavity that is slowly moving toward the outflow boundary.

The final velocity vector plot in Fig. 10 is the steady state result. A pressure contour plot is also given at this time. The cavitation bubble begins slightly downstream of the nose/body intersection point. Since no experimental data is available for this, we

can only state that the results are qualitatively reasonable, exhibiting cavitation where it would be expected.

Steady state results are achieved in this case because the computational region does not include the downstream region where the cavity must eventually close up. Also, the vapor cavity is allowed to pass through the outflow boundary because it is a continuative boundary and not a fixed pressure boundary like that used in the pipe constriction example.

These results are not equivalent to replacing the cavitation bubble with a constant pressure gas bubble. If one tried this, the leading edge of the gas bubble would immediately be swept downstream with the incident flow.

The key difference in the two cases is associated with the flow at the intersection of the torpedo nose and body. In this region, if there is no cavitation, the pressure is reduced below the cavitation pressure because this is the only way flow can be made to turn the corner and satisfy mass continuity (i.e., a zero velocity divergence). When a gas bubble is placed at the corner, the flow separates from the surface but not before turning the flow into the bubble surface and carrying it downstream.

On the other hand, when cavitation is present, flow turns into the vapor bubble with a non-zero velocity divergence. The value of the divergence corresponds to the generation of new vapor which sustains the cavitation bubble.

Cavitation on a Blunt-Nosed Body

In an effort to see how the new model would respond to conditions in which there is only a small localized region of cavitation, a series of calculations were performed for flow over a blunt-nosed body.

Computational Model

The body selected was a cylinder with a hemispherical nose cap. In this case the radius of the cylinder was set at 1.0 in non-dimensional units. The total length of the body included in the computational region was 6.0 units. An inflow boundary was placed 2.0 units in front of the nose.

A unit flow velocity was defined at the inflow boundary and a continuative boundary condition was used at the outflow. To provide a reference pressure, the outer radial boundary at 3.0 units was defined to remain at a constant unit pressure.

The computational mesh had 22 cells in the radial direction with a minimum size of 0.1 at the surface of the cylinder. There were 40 mesh cells used in the axial direction, with a minimum cell size of 0.1 located at the equator of the hemispherical nose.

No Cavitation Results

To provide a benchmark, flow was computed over the body assuming no cavitation, Fig. 11. A minimum pressure of 0.714 was recorded at the junction of the nose with the cylinder. Thus, selecting a cavitation pressure less than this value, or cavitation number K greater the 0.572, will not lead to any cavitation.

Cavitation Results for K=0.56

Setting the cavitation pressure at about 1% above the minimum value observed in the previous computation (P_C=0.72 or K=0.56) should result in a relatively small amount of vapor production. Figure 12 shows the statistically steady result that was computed with the modified FLOW-3D program.

There is a very small cavitation bubble located approximately 0.35 units downstream from the beginning of the cylindrical section of the body. This is in close agreement with one of the photographs (left) shown in Fig. 13, which was taken from Ref. 1. Unfortunately, no data was given in connection with this photograph. The associated text, however, does emphasize that the observed cavitation is slightly downstream from the minimum pressure location, just as observed in the computations.

Our computed results do exhibit some fluctuations in the fluid fraction level at the cavitation location, which indicates that truly steady flow conditions cannot be achieved. This presumably corresponds to the experimental situation in which small bubbles are continuously forming and collapsing in the cavitation zone.

Cavitation Results at K=0.26

For comparison it is interesting to consider what happens when the cavitation pressure is further raised to P_C=0.87 (K=0.26). This value was selected because it corresponds to another photographic result (right) shown in Fig. 13, and reproduced from Batchelor's book, Ref. 6.

In the photograph we see a larger, bubbly cavitation region beginning slightly downstream from the minimum pressure location. The cavitation region has an approximate axial length of 1.5 units. Note also that the nose of the body in the photograph is not hemispherical but more pointed, so we cannot make a direct comparison with the computational example.

Computational results for near steady state conditions are shown in Fig. 14. Here we also see a larger cavitation region, but it is about twice as long as that in the photograph. This difference may be caused by the use of a nose shape that is more blunt and, therefore, more likely to produce more cavitation. In any case, the computed results appear reasonable and do clearly show the increase in cavitation that occurs when the cavitation number is reduced.

Sloshing with Cavitation

The final illustration of a cavitating flow is quite different from the previous cases. Here we wish to examine the effect of cavitation on the sloshing of fluid in an elliptical container under low gravity conditions. Figure 15 is a schematic of the problem. An elliptical tank is half filled with an incompressible liquid (water). For simplicity we shall assume the tank is only two dimensional. A vapor (cavitation) pressure of zero is assigned to the vapor region.

The tank is in a zero-gravity environment but is being subjected to a time-dependent acceleration consisting of two parts. The first part is a constant axial acceleration of -0.1 units (nondimensional) that acts as a low-g body force trying to keep the liquid at the left end of the tank. The second part is sinusoidal with amplitude 0.21 and angular frequency 0.10 radians per time unit.

Computational Model

The tank has been resolved by a mesh consisting of 25 cells in the horizontal direction (direction of acceleration) and 15 cells in the vertical direction. The tank is 100 units in length and 60 units in height.

Noninertial accelerations were modeled using the MOTION routine in FLOW-3D, which is designed for just this purpose. It was necessary, however, to program in the particular acceleration history wanted for this example.

Computational Results

When no cavitation is allowed, the liquid remains at the left end of the tank, Fig. 16, and the axial force exerted on the tank by the liquid simply reflects the applied acceleration. Positive forces in this case, of course, imply negative fluid pressures on the tank wall, a condition that would not be possible with a cavitation pressure of zero.

Figure 17 shows a repeat of the same physical problem except that cavitation has been enabled. After 0.75 cycles of oscillation the fluid has clearly pulled away from the tank wall leaving a vapor cavity. By 1.25 cycles the fluid is located midway in the tank but is heading back toward the left end. Fluid impacts the tank shortly before the 1.75 cycle plot, as can be inferred from the large negative force spike in the force history plot. In the 1.75 cycle picture the liquid has again pulled away from the left wall because negative pressures are not supported in the cavitation model.

A periodic fluid response is not possible in this example because of the large amplitude of the sloshing motion. At the 1.75 cycle plot, for instance, we can see that some liquid has jetted around the tank walls toward the right end of the tank. This simple illustration shows that cavitation phenomena can have important consequences on the hydrodynamic forces generated by sloshing. Here, for instance, the impact of fluid following the collapse of the cavitation bubble generates a force on the tank that is significantly larger than the peak force observed in the no-cavitation case. This happens because there is a large body of fluid (i.e., large momentum) behind the vapor bubble surface that must be brought to rest when the bubble finally collapses. CPU time for this slosh calculation with cavitation was a modest 38.5 minutes (0.64 hours) on a MicroVAX II computer.

SUMMARY AND DISCUSSION

A new model has been added to the FLOW-3D program that permits the investigation of several types of cavitation phenomena. Examples of supercavitation generated by bodies moving through fluids and large cavitation bubbles generated in accelerating containers have been used to illustrate the new model.

Cavitation bubbles are automatically produced in the model when the fluid pressure is at or below the cavitation pressure. Even after their formation, however, we have shown why such bubbles are qualitatively different from constant pressure gas bubbles. We have also seen how the model can be used to gain a better appreciation of the flow dynamics associated with cavitation phenomena.

Experimental data with which to validate the new model is in short supply. Comparisons based on photographic data have been made in this note with good results. As more data becomes available, it will be interesting and fruitful to see how well FLOW-3D can perform. It may be anticipated that computational models of this sort will provide increased understanding of a wide range of important cavitation phenomena.

REFERENCES

1. Arndt, R.E.A., "Cavitation in Fluid Machinery and Hydraulic Structures," Ann. Rev. Fluid Mech. 13, 273 (1981).
2. Suslick, K.S., "The Chemical Effects of Ultrasound," Sci. Am. 260, 80 (Feb. 1989).
3. Sicilian, J.M., Hirt, C.W., and Harper, R.P., "FLOW-3D: Computational Modeling Power for Scientists and Engineers," Flow Science report, FSI-87-00-1 (1987).
4. Hirt, C.W. And Nichols, B.D., "Volume of Fluid (VOF) Method for Dynamics of Free Boundaries," J. Comp. Phys. 39, 201 (1981).
5. Rouse, H., Elementary Mechanics of Fluids, Dover Publications, Inc., NY, reprinted (1978).
6. Batchelor, G.K., An Introduction to Fluid Dynamics, Cambridge Univ. Press, reprinted (1983).

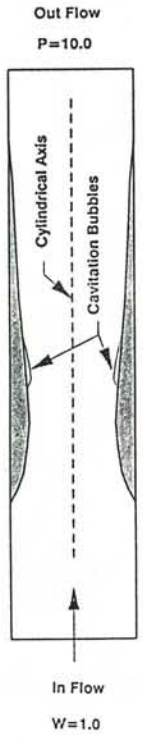

Fig. 1. Schematic for constricted pipe problem.

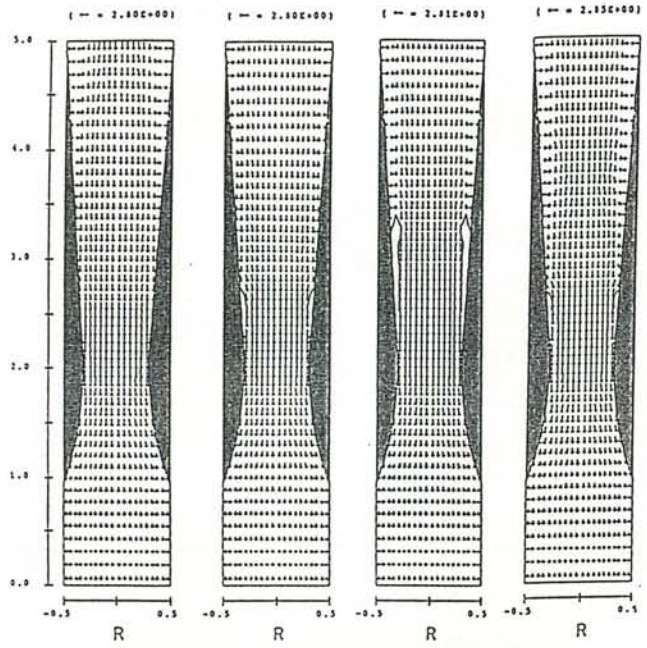

Fig. 2. Evolution of one cycle of cavitation bubble. Times are 9, 11, 13, and 15.

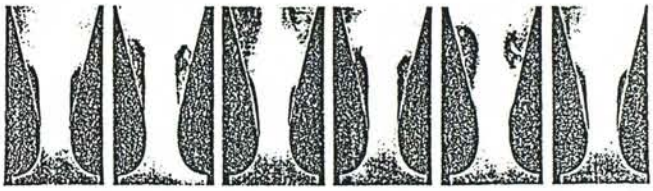

Fig. 3. Frames from motion picture of cavitation at a constriction. Reproduced from Ref. 5.

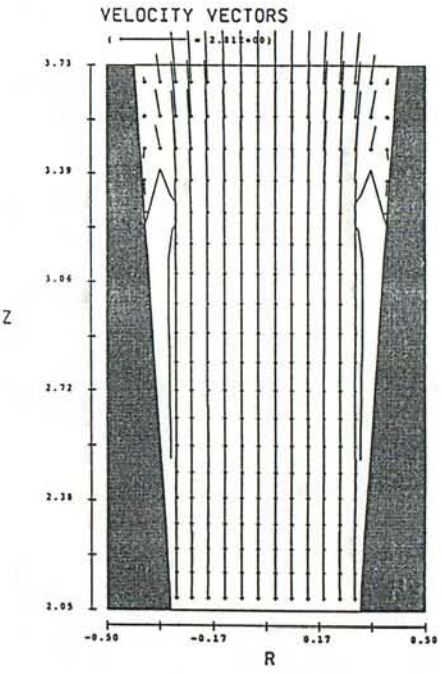

Fig. 4. Closeup of cavity at t=13 showing reversed flow near pipe wall.

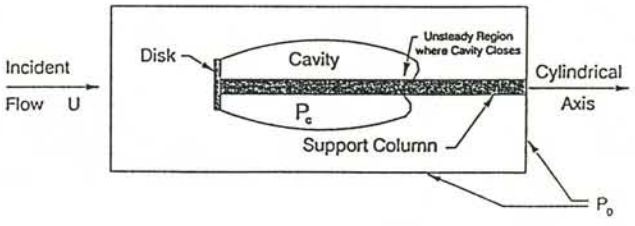

Fig. 5. Schematic of disk problem.

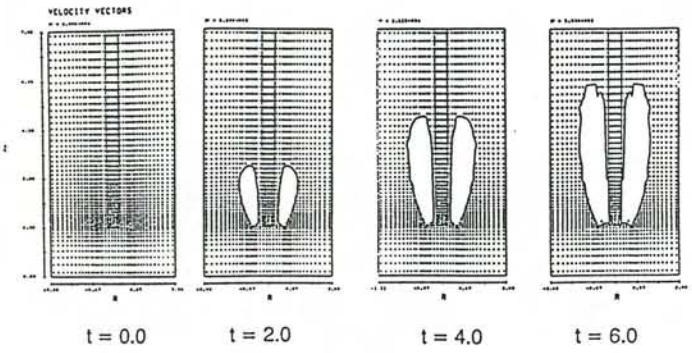

Fig. 6. Time evolution of cavitating wake.

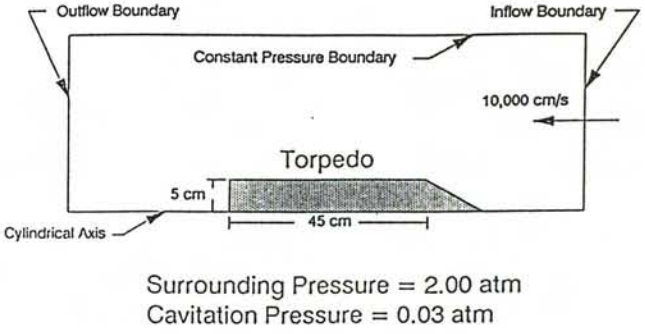

Fig. 9. Schematic of torpedo problem.

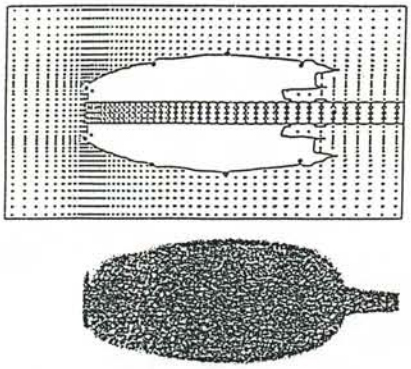

Fig. 7. Comparison with photographic data. Photo (bottom) reproduced from Ref. 6.

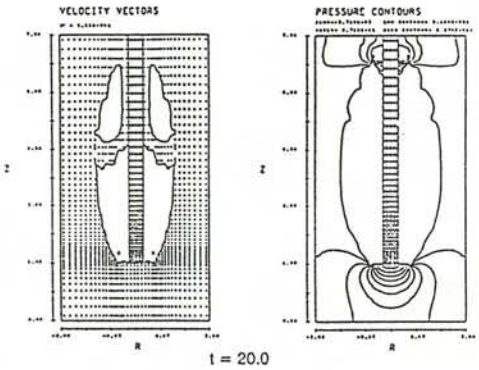

Fig. 8. Computed results at t=20 showing reversed flow at rear of cavity.

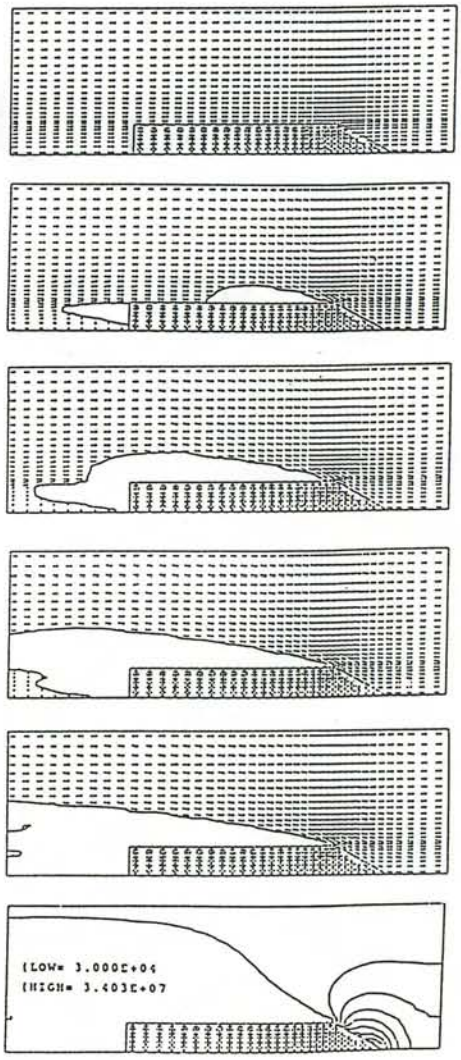

Fig. 10. Time evolution of cavitation. Two bottom frames show steady state conditions (velocities and pressures).

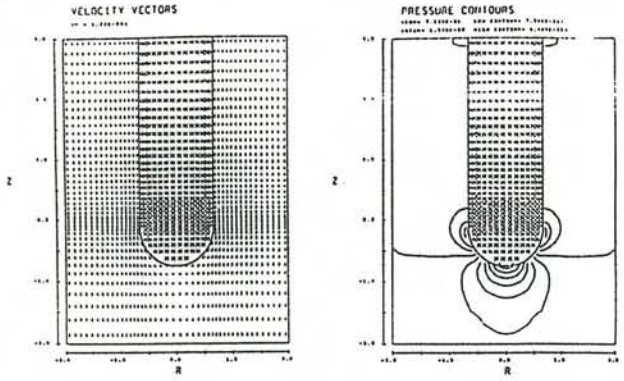

Fig. 11. Flow about blunt cylinder without cavitation.

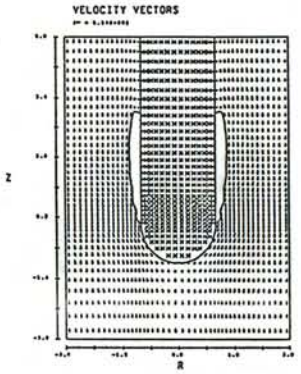

Fig. 14. Flow about blunt cylinder with cavitation, K=0.26.

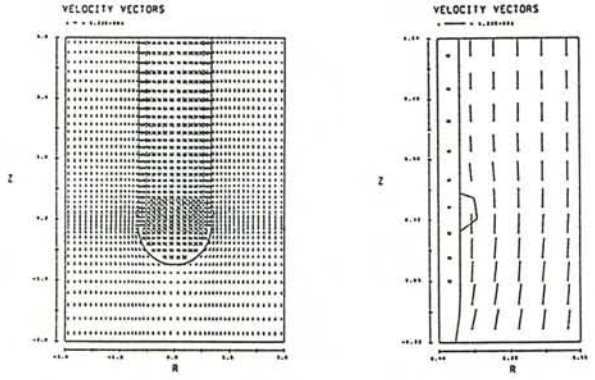

Fig. 12. Flow about blunt cylinder with cavitation, K=0.56. Closeup (right) shows small cavitation bubble.

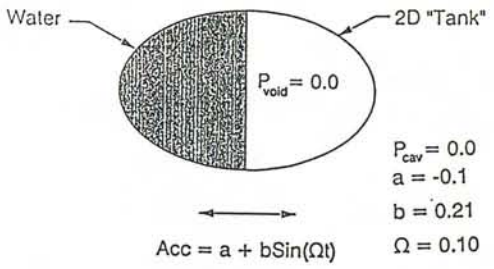

Fig. 15. Schematic for tank acceleration problem.

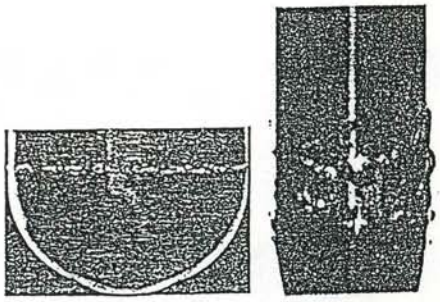

Fig. 13. Experimental photographs of cavitating flows. Left photo from Ref. 1, right photo from Ref. 6.

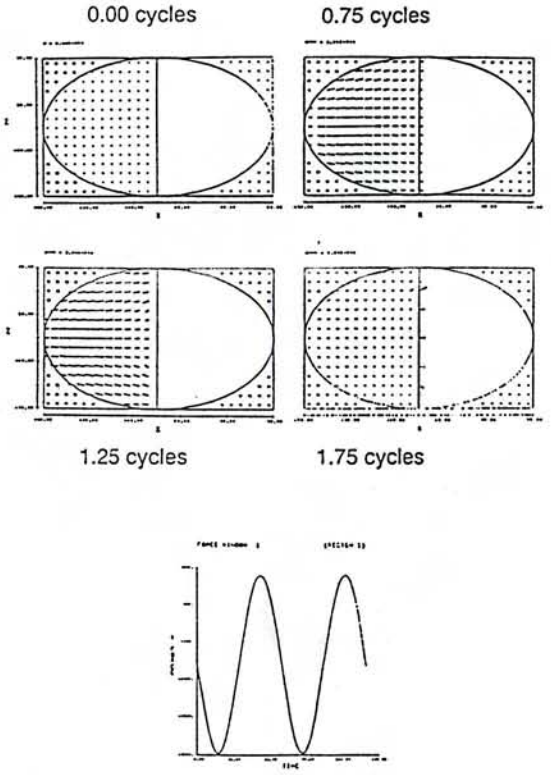

Fig. 16. Results without cavitation.
X force history shown at bottom.

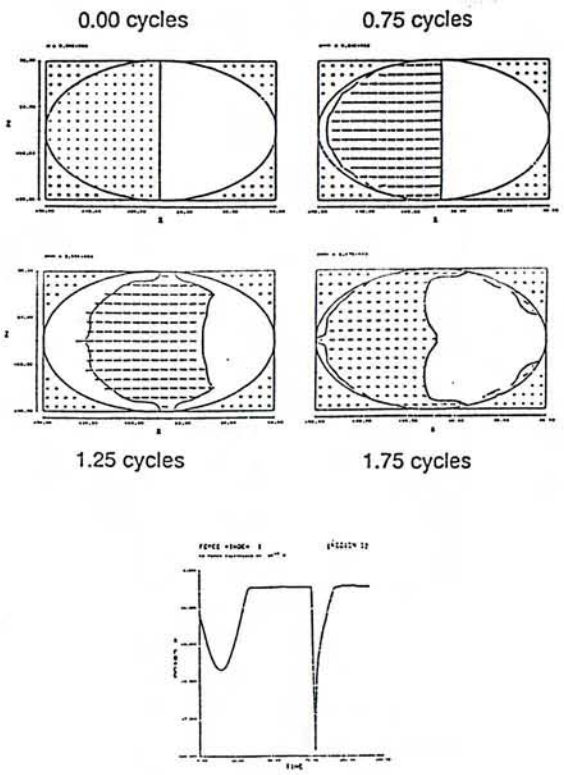

Fig. 17. Results with cavitation.
X force history shown at bottom.